Quantum oscillations of thermopower in WTe_2 thin films

Ran Bi,[1] Zili Feng,[2] Xinqi Li,[1] Jiaji Zhao,[1] Juewen Fan,[1] Youguo Shi,[2,*] Dapeng Yu,[3] and Xiaosong Wu[1,4,†]

[1]*State Key Laboratory for Artificial Microstructure and Mesoscopic Physics, Beijing Key Laboratory of Quantum Devices, Peking University, Beijing 100871, China*

[2]*Institute of Physics and Beijing National Laboratory for Condensed Matter Physics, Chinese Academy of Sciences, Beijing 100190, China*

[3]*Department of Physics, Southern University of Science and Technology of China, Shenzhen 518055, China*

[4]*Collaborative Innovation Center of Quantum Matter, Beijing 100871, China*

(Received 12 June 2019; published 4 December 2019)

Few-layer WTe_2 displays fascinating phenomena, which are believed to be closely related to the topological character of its band structure. In this work we investigate quantum oscillations of thermopower in thin WTe_2 films. Besides four oscillation frequencies commonly observed in bulk materials, we observe an additional oscillation frequency, which has previously been attributed to topological surface states [Nat. Commun. **8**, 2150 (2017)]. Through analysis of the temperature, angular, and film thickness dependence of the frequency, we conclude that it is not due to the cyclotron resonance of the surface Fermi arcs in Weyl semimetals, but rather from the bulk bands. Emergence of these bulk bands at the Fermi level is due to a band reconstruction in thin layers. They contribute to transport and may be responsible for some properties of few-layer WTe_2.

DOI: 10.1103/PhysRevB.100.235405

I. INTRODUCTION

Lately, WTe_2 has attracted a lot of attention because of its extremely large magnetoresistance and its identification as a type-II Weyl semimetal [1–5]. As a van der Waals layered material, it has also been predicted to be a quantum spin Hall insulator in a monolayer limit [6–8]. Extensive efforts on investigating thin films by mechanical exfoliation have been made [9–12]. Very recently, discovery of a few astonishing effects has further enhanced the interest in thin films of this material. Wu *et al.* provided experimental evidence for quantum spin Hall effect in monolayer WTe_2 and found that the effect persists surprisingly up to 100 K [13]. Two groups reported intrinsic superconductivity tuned by carrier density in a monolayer [14,15]. A nonlinear Hall effect due to a nontrivial Berry phase in the absence of an inversion symmetry was discovered in few-layer WTe_2 [16–18]. In combination with the high quality and high mobility, these extraordinary effects showcase WTe_2 as an intriguing platform for studying a variety of topological phenomena.

The main features of the calculated band structure of WTe_2, the starting point of understanding these transport phenomena, have been experimentally confirmed by angle resolved photoemission spectroscopy(ARPES) and quantum oscillations of electrical resistivity [19–22], e.g., a pair of hole (electron) pockets lie symmetrically with respect to the Γ point along the Γ-X direction in the momentum space. Due to inversion symmetry breaking, each is spin-orbit split into two, forming a Russian doll structure [21–23]. However, a pocket at Γ has not been observed by quantum oscillations even though it has been seen in ARPES [19,20]. It is not clear whether this band surfaces to the Fermi level, e.g., in thin films or when gated, hence contributes to some of those experimental observations.

Here we study the quantum oscillations of magnetothermopower (MTEP) in thin films of WTe_2. Since it is the derivative of the conductivity with respect to energy, MTEP exhibits much stronger quantum oscillations than magnetoresistance. We were able to identify and analyze an additional oscillation frequency that is not seen in bulk. Based on the cyclotron mass, thickness, and angular dependence of the frequency, Weyl orbit, a special type of cyclotron orbit consisting of surface Fermi arcs, is ruled out. We show that this frequency is contributed by bulk bands that have shifted to the Fermi level due to a band reconstruction.

II. EXPERIMENTS AND DISCUSSIONS

Single crystals of WTe_2 were grown by a solid state reaction method. The details on the growth and the in-plane transport properties of our samples can be found elsewhere [21,24]. WTe_2 thin film samples were exfoliated from bulk onto a Si wafer with a 285-nm-thick SiO_2 layer. The in-plane crystalline orientations were identified by angle dependent polarized Raman spectroscopy (see the Supplementary Material [25] and Refs. [26,27] therein). Devices were fabricated using the standard e-beam lithography, followed by deposition of 5/50 nm Ti/Au and lift-off. Low temperature transport measurements were carried out using a standard lock-in method in an OXFORD variable temperature cryostat. Thermoelectric effects were measured by employing a lithographically fabricated microstructure, in which a microheater generates a temperature gradient along the sample, as seen in the optical images of two devices in the inset of Figs. 1(a) and 1(d).

When a magnetic field along the $\hat{c}$ axis is applied, quantum oscillations are seen in both magnetoresistance and MTEP,

*ygshi@iphy.ac.cn
†xswu@pku.edu.cn

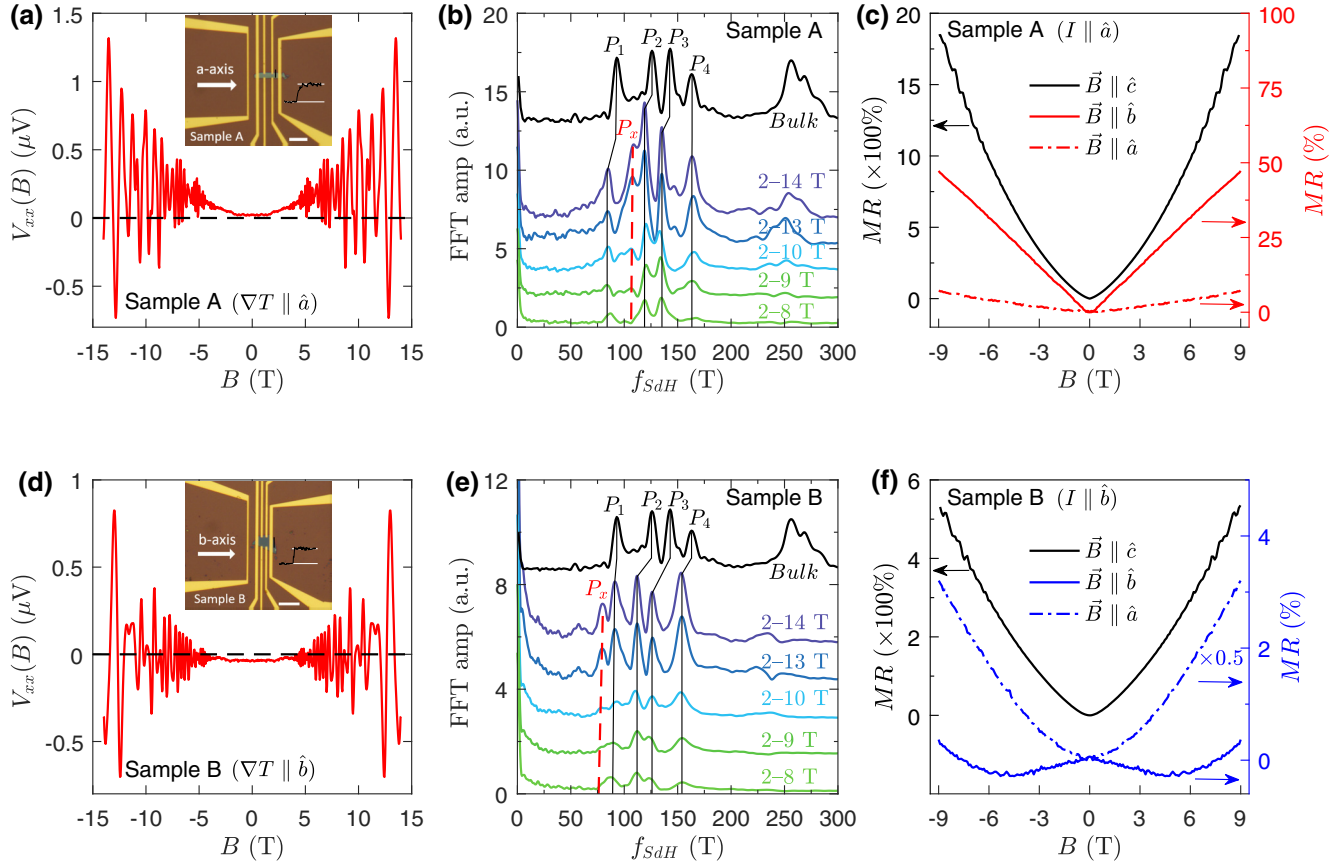

FIG. 1. Quantum oscillations of MTEP and magnetoresistance. (a) MTEP at 1.5 K with the magnetic field along the $\hat{c}$ axis for sample A (21.5 nm thick). The inset shows an optical image of the device with a scale bar representing 10 μm. The thermal gradient is along the $\hat{a}$ axis. (d) MTEP at 1.5 K with the magnetic field along the $\hat{c}$ axis for sample B (14.5 nm thick). The inset shows an optical image of the device. The thermal gradient is along the $\hat{b}$ axis. MTEP for both samples shows pronounced quantum oscillations. (b) and (e) Comparison of fast Fourier transform (FFT) spectra of quantum oscillations between bulk and thin films. The spectrum of the bulk is from magnetoresistance, while the spectra of thin films are from MTEP. FFT is performed for MTEP in different field ranges. An additional oscillation frequency P_x appears when high field data are included. (c) Three MR traces of sample A at 1.5 K ($I \parallel \hat{a}$) with $\vec{B} \parallel \hat{a}$, $\hat{b}$, and $\hat{c}$, respectively. MR is positive in all three configurations. (f) Same as in (c), except it is for sample B ($I \parallel \hat{b}$). Negative longitudinal MR clearly appears in the case of $I \parallel \vec{B} \parallel \hat{b}$ (blue solid line).

shown in Fig. 1. The oscillations in MTEP is much stronger than that in magnetoresistance, which allows their analysis in a much higher resolution. MTEP at low temperatures oscillates around zero, reflecting its nearly perfect electron-hole compensation [1,3,9,21,28,29]. As the thermoelectric power (TEP) is determined by the competition between electron and hole contributions, a slight difference in carrier density of electron and hole can change the sign of TEP. This is the reason why the zero field thermoelectric voltages in samples A and B have opposite signs. To see the oscillation frequencies, fast Fourier transformation (FFT) has been performed. The FFT spectra for field in different ranges are plotted in Figs. 1(b) and 1(e), along with a spectrum of a bulk sample. In both thin flake and bulk samples, four peaks, denoted as P_1–P_4 from low to high frequency, can be identified and are ascribed to four fundamental frequencies corresponding to two pairs of electron (P_2 and P_3) and two pairs of hole (P_1 and P_4) Fermi pockets [9,21,22]. The frequencies are different from those in the bulk sample. This is reasonable, because the oscillation frequency depends on the carrier density, which can vary appreciably in ultrathin flakes due to unintentional surface doping. However, the fact that all four frequencies in thin flakes decrease with respect to the bulk is unexpected, as shifting of the Fermi level would lead to the opposite trend for the size of electron and hole pockets, hence the frequencies. We believe that it indicates change of the band structure. Though the energy bands of WTe_2 preserve the semimetallic property from bulk to trilayer [7,30], the subtle shift in bands may affect the transport properties of thin films [11,12,31]. The most interesting feature is that a new frequency P_x appears near 106.4 T (80.6 T) for sample A (B). Field dependent FFT spectra show that the additional frequency P_x can be observed only when $B > 9$ T both for sample A and B, which clearly separates it from the other four frequencies.

It is tempting to associate this new peak emerging in thin flakes with the quantum oscillations from surface Fermi arcs, as previously done [32]. WTe_2 features Fermi arcs close to the Γ-Y direction on the (001) surface. If Weyl orbits consisting of these surface arcs can form, the frequency of the corresponding quantum oscillations should exhibits a $1/\cos(\theta)$ dependence as the field is tilted away from the $\hat{c}$ axis by an angle of θ. On the other hand, one would expect an ellipsoidal function

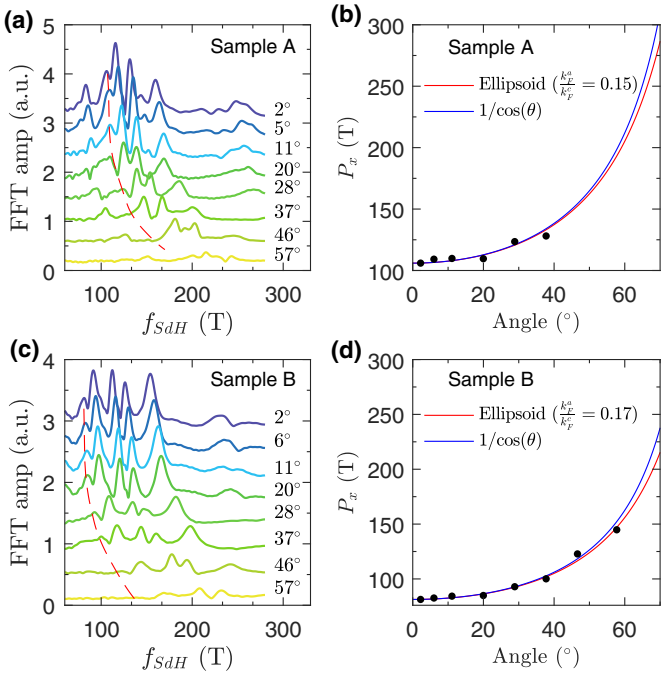

FIG. 2. Angle dependence of quantum oscillations in MTEP at 1.5 K. (a) Angle dependence of the FFT spectra for sample A with field rotated from the $\hat{c}$ axis (0°) to the $\hat{a}$ axis. The red dashed line indicates the evolution of P_x. (b) Angle dependence of the frequency of P_x for sample A. The blue line is a $1/\cos(\theta)$ fit, where θ is the rotation angle. The red line is an ellipsoid fit. (c) FFT spectra for sample B with field rotated from the $\hat{c}$ axis (0°) to the $\hat{a}$ axis. (d) Angle dependence of the frequency of P_x for sample B.

in the simplest case if the oscillation is from bulk band, as occurs for the other four frequencies, P_1–P_4. Figures 2(a) and 2(c) show the FFT spectra from the MTEP oscillations with field rotating from the $\hat{c}$ axis to the $\hat{a}$ axis. The peak position of P_x is plotted as a function of θ in Figs. 2(b) and 2(d). Due to strong suppression of the oscillation with increasing angle, we can only obtain the angular dependence up to 38° for sample A and 58° for sample B. Although $1/\cos(\theta)$ seems to describe the dependence well, an ellipsoidal function works equally well in the limited angle region. So, the angular dependence in our experiment cannot tell whether P_x is from the Weyl orbit or not.

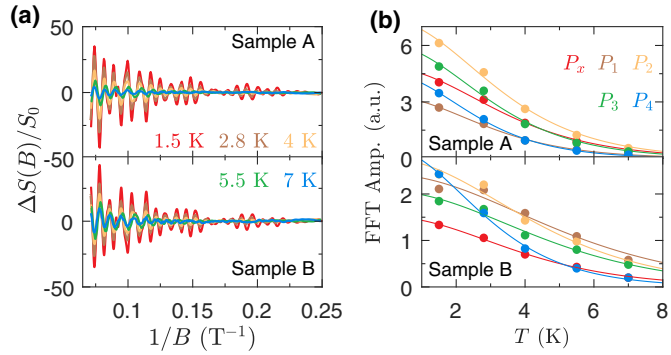

FIG. 3. Temperature dependence of quantum oscillations in MTEP. (a) Oscillation part of MTEP for samples A and B as a function of $1/B$ for various temperatures. (b) FFT amplitudes of oscillations versus temperature for P_x and P_1–P_4. Solid lines are fits to $A(T)$ derived from the Lifshitz-Koservich formula.

We thus extract the cyclotron mass m^* of P_x and compare it with what is expected by the Weyl orbit. We measured the damping of the oscillations with temperature. The temperature dependence of the oscillation amplitude for each frequency is shown in Fig. 3. The oscillations of electrical conductivity are described by the Lifshitz-Kosevich formula, in which the temperature damping factor R_T is used to extract the cyclotron mass [33]. However, quantum oscillations in TEP behave differently as TEP depends on the derivative of the conductivity with respect to energy at the Fermi level. It can be shown that the temperature damping factor of $\Delta S(B)/S_0$ is given by the derivative of R_T, i.e., $A(T) \propto [(\alpha X)\coth(\alpha X) - 1]/[T\sinh(\alpha X)]$, where $\alpha = 2\pi^2 k_B/e\hbar$, $X = m^*T/B$ [34,35]. To obtain the m^* of each Fermi pocket, we have fitted the temperature dependence of the amplitudes of FFT spectra to $A(T)$ in a field range from 4 to 14 T. Table I summarizes the frequency and m^* of P_x and P_1–P_4 for samples A, B, and C. Interestingly, m^* of P_x does not have a clear relationship with the other four frequencies. According to theory, the effective mass $m_{\rm eff}$ of the Weyl orbit is given by $m_{\rm eff} = \hbar k_0/\pi v_{\rm F}^c$, where k_0 is the Fermi-arc length and $v_{\rm F}^c$ is the Fermi velocity along the $\hat{c}$ axis [36]. As the quantum oscillations only exist in a narrow angle range [Figs. 2(c) and 2(d)], $v_{\rm F}^c$ of WTe_2 thin flake is approximated from the bulk one with a value of 2.5×10^5 m/s [23]. In this way, $m_{\rm eff}$ is estimated as 0.048 m_e,

TABLE I. The frequency and effective mass (m^*) of P_x and P_1–P_4 for samples A, B, and C.

Sample A	P_x	P_1	P_2	P_3	P_4
Frequency (T)	106.4 ± 5.0	86.3 ± 3.3	117.6 ± 4.2	134.4 ± 1.5	162.4 ± 4.9
m^* (m_e)	0.27 ± 0.02	0.32 ± 0.02	0.29 ± 0.02	0.30 ± 0.01	0.36 ± 0.02
Sample B	P_x	P_1	P_2	P_3	P_4
Frequency (T)	80.6 ± 4.2	91.0 ± 4.2	112.0 ± 4.2	126.0 ± 3.5	151.7 ± 4.7
m^* (m_e)	0.24 ± 0.02	0.21 ± 0.02	0.22 ± 0.02	0.21 ± 0.02	0.32 ± 0.01
Sample C	P_x	P_1	P_2	P_3	P_4
Frequency (T)	48.7 ± 3.4	81.9 ± 3.5	103.4 ± 4.7	118.7 ± 2.7	133.0 ± 3.2
m^* (m_e)	0.24 ± 0.02	0.23 ± 0.01	0.23 ± 0.01	0.27 ± 0.01	0.30 ± 0.02

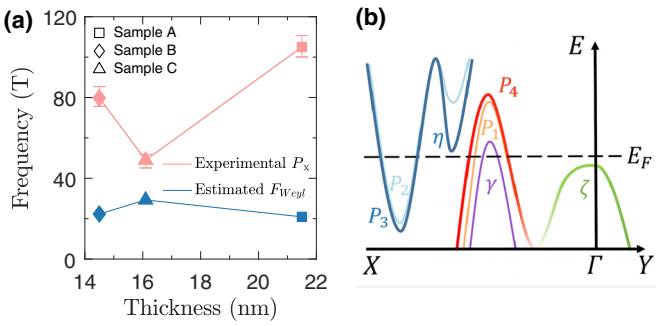

FIG. 4. Origin of P_x. (a) Expected oscillation frequency of the Weyl orbit F_{Weyl} and the actual frequency P_x as a function of thickness. (b) A schematic representation of the band structure of γ, η, ζ, and P_1–P_4 near the Fermi level. The figure is not drawn to scale.

where k_0 is obtained from Ref. [20] as 0.32 nm^{-1}. This value of m_{eff} is much smaller than that of P_x shown in Table I, which suggests that P_x is not due to the Weyl orbit.

The quantum oscillation frequency of the Weyl orbit is determined by the length of the Fermi arc, $F_{\text{Weyl}} = E_{\text{F}}k_0/e\pi v_{\text{F}}^c$, where E_{F} is the bulk Fermi level [36]. The bulk oscillation frequency and effective mass when field along the $\hat{c}$ axis provide direct access to the Fermi level $E_F = (\hbar k_F)^2/2m^* =$ 51.6 meV for sample A. The frequency of the Weyl orbit is estimated as $F_{\text{Weyl}} = 20.9$ T. Experimentally, the frequency for P_x varies significantly in different samples, from 48.7 to 106.4 T, as shown in Table I. In contrast, the calculated F_{Weyl} for different samples, plotted in Fig. 4(a) by blue, shows a weak relation with thickness. The strong sample-to-sample dependence of the frequency is difficult to understand under the picture of the Weyl orbit.

These observations lead us to believe that P_x is not originated from the Weyl orbit. In WTe_2, the Fermi arcs appear on the (001) surface, but not on the (100) or (010) surface [4,5,37]. Therefore, to form a Weyl orbit, the magnetic field has to have a component in the $\hat{c}$ direction. On the other hand, the Weyl orbit requires a gapless chiral Landau level in the bulk, through which electrons can transport from one surface to the other, completing a close orbit. Although such a chiral Landau level can exist in type-I Weyl semimetals, no matter what direction the field is along, it is limited for field direction in a certain range for type-II Weyl semimetals. In WTe_2, the field needs to be close to the direction of the $\hat{b}$ axis [4]. This condition has been experimentally demonstrated by magnetoresistance. Only when the field is close to the $\hat{b}$ axis, negative magnetoresistance induced by the chiral anomaly, which stems from the chiral Landau level, appears. This is also what we observed in our samples. As shown in Figs. 1(c) and 1(f), the magnetoresistance is negative only when $\vec{B} \parallel I \parallel \hat{b}$, while it remains positive for all other geometric configurations. Combining these two requirements, one concludes that the Weyl orbit emerges when the field is slightly tilted away from the direction of the $\hat{b}$ axis. Thus, P_x we observed when $\vec{B} \parallel \hat{c}$ does not come from the Weyl orbit.

We now discuss the possible origin of P_x. Since P_x appears in high fields, one possibility is that it is due to magnetic breakdown. In bulk materials, oscillations induced by magnetic breakdown has been observed in thermopower owing to their high mobility, but they are at frequencies much higher than P_1–P_4 [21]. Moreover, we are not able to construct a reasonable magnetic breakdown orbit that produces P_x. Therefore, P_x must originate from another band. This band has a mean free time shorter than that in P_1–P_4, so P_x occurs in high fields [38]. In previous ARPES and calculation studies on the band structure of bulk WTe_2, there are three bands in the vicinity of the Fermi level [19,20,39]. The electron band is referred to as η, and the two hole bands are referred to as ζ and γ. Electrical transport experiments on bulk have not seen them, likely because the tops (bottoms) of these bands are slightly below (above) the Fermi level. In thin flake samples, it is possible that one of these bands may cross the Fermi level and produce an additional oscillation frequency due to shifting of the Fermi level and/or the band reconstruction we mentioned earlier in this work. In Fig. 4(b) a schematic diagram of the band structure near the Fermi level is proposed. We believe that P_x is most likely attributed to the bulk γ and η band based on the following evidence.

First, the Γ point is a high symmetry point, around which the ζ band is nearly degenerated. Meanwhile, the strong spin-orbit coupling in WTe_2 splits the degenerate bands along Γ-X. The large split in the γ and η band leads to a single pocket crossing the Fermi level [39]. Thus, only one additional frequency appears in quantum oscillations. In contrast, the electron bands (P_2, P_3) and hole bands (P_1, P_4) appear in pairs, as a result of spin splitting by spin-orbit coupling in the absence of inversion symmetry [4,22,23].

Second, these three bands are close in energy [20,40]. So, a small shift in the Fermi level can cause different hole or electron bands to intersect the Fermi level, resulting in an additional oscillation frequency. Since the Fermi level of ultrathin materials is susceptible to unintentional surface doping, it is not surprising that the oscillation frequencies vary from sample to sample. The strong variation of the P_x frequency implies involvement of more than one band. ARPES studies have indicated that the ζ band is a flat band, suggesting a relatively larger effective mass than that of P_1–P_4 [20], whereas the effective mass of P_x is found to be similar to others, shown in Table I. So the ζ band is excluded and the plausible origin of P_x would be the γ and η bands.

The observation that the Fermi surfaces for both the hole and electron bands, manifested as P_1, P_4 and P_2, P_3, shrink in thin samples cannot be accounted for by a mere change of the Fermi level. It indicates a band shift, e.g., a reduction of the overlap in energy between the hole and electron bands. This behavior, predicted by theoretical calculations [12,41], naturally explains the emergence of other bands at the Fermi level, which are near the Fermi level in bulk samples. The band reconstruction in ultrathin van der Waals materials is commonly seen. For instance, it is well known that certain transition metal dichalcogenides, such as WS_2, WSe_2, MoS_2, change from an indirect semiconductor to a direct one with decreasing thickness [42–45]. The change of the electronic structure with thickness may be attributed to various mechanisms, such as quantum confinement effects, symmetry breaking, or lattice relaxation [30,42,43,46]. The effect of the lattice relaxation on the band structure is particularly strong

in materials whose band structure is sensitively dependent of the lattice constants. WTe_2 and $ZrTe_5$ are examples where a slight change of the lattice constant due to thermal expansion is sufficient to substantially modify the band. A temperature-induced Lifshitz transition has been observed in both materials [39,47,48]. Subsequently, it has been realized that their characteristic electrical transport features are closely related to the transition. Furthermore, when the thickness is reduced to a monolayer, the lattice structure of WTe_2 is predicted to evolve from $1T_d$ to $1T'$, which gives rise to a topological transition of the band structure [13,41]. This evolution has been confirmed in epitaxial thin film and surface layers of bulk crystal [8,30]. In light of these possibilities, the observation presented in this work can be easily understood. Our results indicate that it is crucial to consider the band reconstruction in order to understand the electrical transport of ultrathin WTe_2.

At last, it is worth discussing the possibility of a strain effect in our devices deposited on a SiO_2/Si substrate. It is known that in some monolayer materials, MoS_2 for example, substrate-induced strain can reduce the band gap and shift the relative position between different bands [49,50]. However, the modification of the band structure by the substrate-induced strain is much weaker in multilayer than in monolayer [51]. In addition, Raman spectra have shown no difference between suspended and supported WTe_2 flakes with thickness up to eight layers, which indicates that the substrate-induced strain, if any, has little impact on the atomic vibration and lattice symmetries [52]. Thus, the strain effects in our devices is negligible.

III. CONCLUSIONS

To summarize, magnetothermoelectric measurements were performed for WTe_2 thin films along two in-plane crystal directions and of various thicknesses. Quantum oscillations of MTEP, much stronger than that of magnetoresistance, are observed and an additional oscillation frequency is revealed. Through detailed study of the thickness and angular dependence of the frequency and the associated cyclotron mass, we conclude that it is not from the cyclotron of the Weyl orbit, but from the bulk bands that were in close proximity to the Fermi level. Moreover, the comparison between the oscillation frequencies of bulk and those of thin films suggests a shift of energy between the bands when the thickness is reduced. The emergence of other bands near the Fermi level underlines their potentially important role in electric transport in thin films of WTe_2.

ACKNOWLEDGMENTS

This work was supported by National Key Basic Research Program of China (No. 2016YFA0300600) and NSFC (Projects No. 11574005 and No. 11774009).

[1] M. N. Ali, J. Xiong, S. Flynn, J. Tao, Q. D. Gibson, L. M. Schoop, T. Liang, N. Haldolaarachchige, M. Hirschberger, N. P. Ong, and R. J. Cava, Nature (London) **514**, 205 (2014).
[2] Y. Zhao, H. Liu, J. Yan, W. An, J. Liu, X. Zhang, H. Wang, Y. Liu, H. Jiang, Q. Li, Y. Wang, X.-Z. Li, D. Mandrus, X. C. Xie, M. Pan, and J. Wang, Phys. Rev. B **92**, 041104(R) (2015).
[3] P. L. Cai, J. Hu, L. P. He, J. Pan, X. C. Hong, Z. Zhang, J. Zhang, J. Wei, Z. Q. Mao, and S. Y. Li, Phys. Rev. Lett. **115**, 057202 (2015).
[4] A. A. Soluyanov, D. Gresch, Z. Wang, Q. Wu, M. Troyer, X. Dai, and B. A. Bernevig, Nature (London) **527**, 495 (2015).
[5] Y. Wang, E. Liu, H. Liu, Y. Pan, L. Zhang, J. Zeng, Y. Fu, M. Wang, K. Xu, Z. Huang, Z. Wang, H.-Z. Lu, D. Xing, B. Wang, X. Wan, and F. Miao, Nat. Commun. **7**, 13142 (2016).
[6] X. Qian, J. Liu, L. Fu, and J. Li, Science **346**, 1344 (2014).
[7] Z. Fei, T. Palomaki, S. Wu, W. Zhao, X. Cai, B. Sun, P. Nguyen, J. Finney, X. Xu, and D. H. Cobden, Nat. Phys. **13**, 677 (2017).
[8] S. Tang, C. Zhang, D. Wong, Z. Pedramrazi, H.-Z. Tsai, C. Jia, B. Moritz, M. Claassen, H. Ryu, S. Kahn, J. Jiang, H. Yan, M. Hashimoto, D. Lu, R. G. Moore, C.-C. Hwang, C. Hwang, Z. Hussain, Y. Chen, M. M. Ugeda, Z. Liu, X. Xie, T. P. Devereaux, M. F. Crommie, S.-K. Mo, and Z.-X. Shen, Nat. Phys. **13**, 683 (2017).
[9] L. Wang, I. Gutierrez-Lezama, C. Barreteau, N. Ubrig, E. Giannini, and A. F. Morpurgo, Nat. Commun. **6**, 8892 (2015).
[10] J. Na, A. Hoyer, L. Schoop, D. Weber, B. V. Lotsch, M. Burghard, and K. Kern, Nanoscale **8**, 18703 (2016).
[11] V. Fatemi, Q. D. Gibson, K. Watanabe, T. Taniguchi, R. J. Cava, and P. Jarillo-Herrero, Phys. Rev. B **95**, 041410(R) (2017).
[12] F.-X. Xiang, A. Srinivasan, Z. Z. Du, O. Klochan, S.-X. Dou, A. R. Hamilton, and X.-L. Wang, Phys. Rev. B **98**, 035115 (2018).
[13] S. Wu, V. Fatemi, Q. D. Gibson, K. Watanabe, T. Taniguchi, R. J. Cava, and P. Jarillo-Herrero, Science **359**, 76 (2018).
[14] V. Fatemi, S. Wu, Y. Cao, L. Bretheau, Q. D. Gibson, K. Watanabe, T. Taniguchi, R. J. Cava, and P. Jarillo-Herrero, Science **362**, 926 (2018).
[15] E. Sajadi, T. Palomaki, Z. Fei, W. Zhao, P. Bement, C. Olsen, S. Luescher, X. Xu, J. A. Folk, and D. H. Cobden, Science **362**, 922 (2018).
[16] Q. Ma, S.-Y. Xu, H. Shen, D. MacNeill, V. Fatemi, T.-R. Chang, A. M. Mier Valdivia, S. Wu, Z. Du, C.-H. Hsu, S. Fang, Q. D. Gibson, K. Watanabe, T. Taniguchi, R. J. Cava, E. Kaxiras, H.-Z. Lu, H. Lin, L. Fu, N. Gedik, and P. Jarillo-Herrero, Nature (London) **565**, 337 (2018).
[17] K. Kang, T. Li, E. Sohn, J. Shan, and K. F. Mak, Nat. Mater. **18**, 324 (2019).
[18] S.-Y. Xu, Q. Ma, H. Shen, V. Fatemi, S. Wu, T.-R. Chang, G. Chang, A. M. M. Valdivia, C.-K. Chan, Q. D. Gibson, J. Zhou, Z. Liu, K. Watanabe, T. Taniguchi, H. Lin, R. J. Cava, L. Fu, N. Gedik, and P. Jarillo-Herrero, Nat. Phys. **14**, 900 (2018).
[19] J. Jiang, F. Tang, X. C. Pan, H. M. Liu, X. H. Niu, Y. X. Wang, D. F. Xu, H. F. Yang, B. P. Xie, F. Q. Song, P. Dudin, T. K. Kim, M. Hoesch, P. K. Das, I. Vobornik, X. G. Wan, and D. L. Feng, Phys. Rev. Lett. **115**, 166601 (2015).
[20] C. Wang, Y. Zhang, J. Huang, S. Nie, G. Liu, A. Liang, Y. Zhang, B. Shen, J. Liu, C. Hu, Y. Ding, D. Liu, Y. Hu, S. He, L. Zhao, L. Yu, J. Hu, J. Wei, Z. Mao, Y. Shi, X. Jia, F. Zhang,

S. Zhang, F. Yang, Z.Wang, Q. Peng, H.Weng, X. Dai, Z. Fang, Z. Xu, C. Chen, and X. J. Zhou, Phys. Rev. B **94**, 241119(R) (2016).

[21] Z. Zhu, X. Lin, J. Liu, B. Fauqué, Q. Tao, C. Yang, Y. Shi, and K. Behnia, Phys. Rev. Lett. **114**, 176601 (2015).

[22] D. Rhodes, S. Das, Q. R. Zhang, B. Zeng, N. R. Pradhan, N. Kikugawa, E. Manousakis, and L. Balicas, Phys. Rev. B **92**, 125152 (2015).

[23] R. Bi, Z. Feng, X. Li, J. Niu, J. Wang, Y. Shi, D. Yu, and X. Wu, New J. Phys. **20**, 063026 (2018).

[24] D. Kang, Y. Zhou, W. Yi, C. Yang, J. Guo, Y. Shi, S. Zhang, Z. Wang, C. Zhang, S. Jiang, A. Li, K. Yang, Q. Wu, G. Zhang, L. Sun, and Z. Zhao, Nat. Commun. **6**, 7804 (2015).

[25] See Supplemental Material at http://link.aps.org/supplemental/10.1103/PhysRevB.100.235405 for polarized Raman scattering spectra and additional thermopower data.

[26] Q. Song, X. Pan, H. Wang, K. Zhang, Q. Tan, P. Li, Y. Wan, Y. Wang, X. Xu, M. Lin, X. Wan, F. Song, and L. Dai, Sci. Rep. **6**, 29254 (2016).

[27] B. J. Thaler and J. Bass, J. Phys. F: Met. Phys **5**, 1554 (1975).

[28] H. Y. Lv, W. J. Lu, D. F. Shao, Y. Liu, S. G. Tan, and Y. P. Sun, Europhys. Lett. **110**, 37004 (2015).

[29] Y. Wang, L. Wang, X. Liu, H. Wu, P. Wang, D. Yan, B. Cheng, Y. Shi, K. Watanabe, T. Taniguchi, S.-J. Liang, and F. Miao, Nano Lett. **19**, 3969 (2019).

[30] P. K. Das, D. Di Sante, I. Vobornik, J. Fujii, T. Okuda, E. Bruyer, A. Gyenis, B. E. Feldman, J. Tao, R. Ciancio, G. Rossi, M. N. Ali, S. Picozzi, A. Yadzani, G. Panaccione, and R. J. Cava, Nat. Commun. **7**, 10847 (2016).

[31] Y. Chen, B. Peng, C. Cong, J. Shang, L. Wu, W. Yang, J. Zhou, P. Yu, H. Zhang, Y. Wang, C. Zou, J. Zhang, S. Liu, Q. Xiong, H. Shao, Z. Liu, H. Zhang, W. Huang, and T. Yu, Adv. Mater. **31**, 1804979 (2019).

[32] P. Li, Y. Wen, X. He, Q. Zhang, C. Xia, Z.-M. Yu, S. A. Yang, Z. Zhu, H. N. Alshareef, and X.-X. Zhang, Nat. Commun. **8**, 2150 (2017).

[33] D. Shoenberg, *Magnetic Oscillations in Metals*, Cambridge Monographs on Physics (Cambridge University Press, Cambridge, 1984).

[34] R. Fletcher, J. Phys. F: Met. Phys **11**, 1093 (1981).

[35] A. Palacio Morales, A. Pourret, G. Knebel, G. Bastien, V. Taufour, D. Aoki, H. Yamagami, and J. Flouquet, Phys. Rev. B **93**, 155120 (2016).

[36] A. C. Potter, I. Kimchi, and A. Vishwanath, Nat. Commun. **5**, 5161 (2014).

[37] Y. Wu, D. Mou, N. H. Jo, K. Sun, L. Huang, S. L. Bud'ko, P. C. Canfield, and A. Kaminski, Phys. Rev. B **94**, 121113(R) (2016).

[38] In principle, the mean free time can be estimated from the oscillation of individual frequencies via the Dingle plot. However, such an estimation becomes unreliable due to the overlap between different frequencies. See some attempts and corresponding discussion in the Supplementary Material [25] and Ref. [27] therein.

[39] Y. Wu, N. H. Jo, M. Ochi, L. Huang, D. Mou, S. L. Bud'ko, P. C. Canfield, N. Trivedi, R. Arita, and A. Kaminski, Phys. Rev. Lett. **115**, 166602 (2015).

[40] Y. Wu, N. H. Jo, D. Mou, L. Huang, S. L. Bud'ko, P. C. Canfield, and A. Kaminski, Phys. Rev. B **95**, 195138 (2017).

[41] F. Zheng, C. Cai, S. Ge, X. Zhang, X. Liu, H. Lu, Y. Zhang, J. Qiu, T. Taniguchi, K. Watanabe, S. Jia, J. Qi, J.-H. Chen, D. Sun, and J. Feng, Adv. Mater. **28**, 4845 (2016).

[42] K. F. Mak, C. Lee, J. Hone, J. Shan, and T. F. Heinz, Phys. Rev. Lett. **105**, 136805 (2010).

[43] A. Splendiani, L. Sun, Y. Zhang, T. Li, J. Kim, C.-Y. Chim, G. Galli, and F. Wang, Nano Lett. **10**, 1271 (2010).

[44] W. S. Yun, S. W. Han, S. C. Hong, I. G. Kim, and J. D. Lee, Phys. Rev. B **85**, 033305 (2012).

[45] Y. Sun, D. Wang, and Z. Shuai, J. Phys. Chem. C **120**, 21866 (2016).

[46] V. Tran, R. Soklaski, Y. Liang, and L. Yang, Phys. Rev. B **89**, 235319 (2014).

[47] Y. Zhang, C. Wang, L. Yu, G. Liu, A. Liang, J. Huang, S. Nie, X. Sun, Y. Zhang, B. Shen, J. Liu, H. Weng, L. Zhao, G. Chen, X. Jia, C. Hu, Y. Ding, W. Zhao, Q. Gao, C. Li, S. He, L. Zhao, F. Zhang, S. Zhang, F. Yang, Z. Wang, Q. Peng, X. Dai, Z. Fang, Z. Xu, C. Chen, and X. J. Zhou, Nat. Commun. **8**, 15512 (2017).

[48] F. C. Chen, H. Y. Lv, X. Luo, W. J. Lu, Q. L. Pei, G. T. Lin, Y. Y. Han, X. B. Zhu, W. H. Song, and Y. P. Sun, Phys. Rev. B **94**, 235154 (2016).

[49] H. Jeong, H. M. Oh, A. Gokarna, H. Kim, S. J. Yun, G. H. Han, M. S. Jeong, Y. H. Lee, and G. Lerondel, Adv. Mater. **29**, 1700308 (2017).

[50] J. T. Mlack, P. Masih Das, G. Danda, Y.-C. Chou, C. H. Naylor, Z. Lin, N. P. López, T. Zhang, M. Terrones, A. T. C. Johnson, and M. Drndić, Sci. Rep. **7**, 43037 (2017).

[51] Y. C. Jiang, J. Gao, and L. Wang, Sci. Rep. **6**, 19624 (2016).

[52] J. Lee, F. Ye, Z. Wang, R. Yang, J. Hu, Z. Mao, J. Wei, and P. X.-L. Feng, Nanoscale **8**, 7854 (2016).